Chapter

Memristor Behavior under Dark and Violet Illumination in Thin Films of ZnO/ZnO-Al Multilayers

Adolfo Henrique Nunes Melo, Raiane Sodre de Araujo, Eduardo Valença and Marcelo Andrade Macêdo

Abstract

ZnO/ZnO-Al thin films were grown aiming the development of a memristor. Electrical voltage sweeps were imposed to induce dopant migration and to achieve several resistance states. A memristor behavior was observed, presenting adaptation to external electrical stimulus. Voltage sweeps occurred under the influence of violet light and in the dark, alternately, and the influence of the photon incidence on the current intensity was noticed. Throughout the alternating cycles between light and dark, less resistance was observed under illumination, but the migration of Al and O ions caused the formation of Al_2O_3 and ZnO oxides, resulting in a gradual increase in resistance. With constant voltage, the device presented continuous modification of resistance and sensitivity to the violet light with generation of free carriers. These results bring new opportunities for using memristors as violet light sensors as well as new insights for light-controlled memristor development.

Keywords: memristor, ZnO, ZnO-Al, thin films, violet sensor, dark, illumination, memristive behavior

1. Introduction

In 1971, Leon Chua predicted the existence of a fourth electronic passive element of two terminals, called a memristor (a union of the terms memory and resistance) [1]. A memristor is basically a resistor that has its resistance altered with external stimulation in a nonvolatile way. In other words, it maintains the state of resistance even if the stimulus is removed. In 1976, Chua and Kang determined that a wide class of devices and systems can be considered as memristives when they present time-dependent electrical resistance and also depend on application of electric voltage [2]. Memristor devices can be configured in nonvolatile memories, logic gates, and programmable connections having high-density integration or presenting complementary metal-oxide-semiconductor (CMOS) compatibility [3]. This CMOS compatibility makes memristors excellent candidates to go beyond Moore's law.

In 2008, in Hewlett-Packard (HP) laboratories, thin films of titanium dioxide prepared with two terminals presented memristor characteristics [4]. Their basic structure was based on epitaxial growth of metal-insulator-metal (MIM) thin

films [5–7]. With the experimental development of memristors in HP laboratories, there has been increasing research in this area, and several materials have been constructed in the MIM structure for analysis of memristive behavior. There is an appreciable number of materials that have been applied in the design of the MIM structure, such as semiconductor insulation (III-V), including MgO, TiO_x, ZrO_x, HfO_x, NbO_x, AlO_x, ZnO_x, or rare-earth oxides containing Y, Ce, Sm, Gd, Eu, Nd, and perovskites ($SrTiO_3$, $Ba_{0.7}Sr_{0.3}TiO_3$) [8, 9]. In addition to such applications as nonvolatile memory, devices based on transparent memristors can be applied even in near-eye display technology that requires the construction of transparent memories, transparent switches, and optical sensors [10]. These devices can also act as synapse elements, creating neural computing machines resembling the behavior of the biological brain [7, 11, 12].

However, transparent conductive oxides (TCOs) have been widely studied because they are essential components in flat-panel monitors, solar cells, touch screens, light-emitting diodes (LEDs), ultraviolet (UV) detectors, and other optoelectronic devices [10, 13, 14]. In addition, new transparent devices are being developed in applications of neuromorphic circuits [4, 7, 15] and adaptive systems [16, 17] in which they are based on resistive commutation depending on the history of the electric voltage application. Among the various materials that have memristor characteristics, ZnO stands out for its low toxicity, low cost, wide resistive switching ratio (R_{off}/R_{on} ~10^{11}), low power consumption, fast recording, and high-density storage [5, 10, 18, 19]. For the construction of a transparent MIM system, an indium tin oxide (ITO) substrate can be used because of its optical properties (transmittance ~90%) and electrical properties (sheet resistance ~20 Ω/sq) [20]. Transparent thin films of ZnO have been extensively studied which acquires excellent optical and electrical properties when doped with such metals as Al [21], Ti [22], and Nb [13], but a multilayer insulator/insulator+metal system may be a good candidate for memristor characteristics, where the diffusion of metallic ions may favor the mechanism of adaptation to the external electrical stimulus. Some researchers have reported thin films of ZnO/ZnO:Al presenting optical transmission of $> 80\%$ and bandgap $E_g = 3.32\,eV$ [23] or ranging from 3.65 to 3.72 eV when grown under heat treatment (300–500°C) [24].

Bandgap studies have an important role for light detection (near the ultraviolet UV zone in the case of ZnO), biological and environmental research, and detection sensors, being a protagonist in several chemical processes, which makes its determination extremely important. Bandgap determination can favor the development of wavelength-sensitive circuits enabling the generation of electrical signals that can be measured. However, memristive systems require electric charge flux through the device, which causes variation in the internal electrical resistance. This can be controlled using light incidence in addition to the usual electrical voltage. Inspired by the biological processes, Chen et al. demonstrated a visual memory unit in which it was based on In_2O_3 resistive switching, where logic states (0) and (1) associated with the high-resistance state and low-resistance state, respectively, were achieved under dark and UV illumination conditions, where the existence of UV stimulation provides the possibility of light information being memorized and erased under voltage sweep and then records light patterns, such as butterfly or heart shaped, in arrangements of 10 × 10 pixels [25].

In this work, ITO/ZnO/ZnO-Al memristor devices were grown using magnetron sputtering. They were subjected to electrical voltage sweep to study homogeneous resistive switching behavior under illumination and dark ambient conditions. The analysis of optical transmission and absorption properties and bandgap determination are also presented.

2. Experimental details

Thin films of ZnO/ZnO-Al were deposited on substrates of 100-nm Asahi Glass indium tin oxide (ITO) through physical deposition system RF/DC magnetron sputtering (AJA International). Three samples of ZnO thin films were grown on ITO using 100-W RF applied to a ceramic target of ZnO (99.9% purity, Macashew Technologies) as a function of the deposition time (40, 60, and 100 min). On these samples, a ZnO-Al film was grown by codeposition for 15 min, where an Al target (98.8%) was exposed to a 50 W DC source and simultaneously the ZnO target to 100 W RF. In all depositions, the base pressure was ~10^{-6} Torr, and the working pressure with Ar gas was 20 mTorr with continuous flux of 20 sccm. There was no supply of oxygen flow, and all depositions were without heating source. The samples in this case had an epitaxial architecture. For simplicity, coding was performed, where ZA1 refers to the sample ITO/ZnO(100 min)/ZnO-Al(15 min), ZA2 refers to ITO/ZnO(60 min)/ZnO-Al(15 min), and ZA3 to ITO/ZnO(40 min)/ZnO-Al(15 min). The crystallinity of the samples was analyzed by X-ray diffraction (Bruker D8 Advance—CuK_α radiation with $\lambda = 0.154$ nm). A concentration profile of chemicals per depth was obtained through the Rutherford backscattering spectroscopy (RBS) technique carried out by bombardment of He^+ (2.2 MeV). The RBS data were obtained simultaneously at 120° and 170° scattering angles. This methodology was applied previously for the fabrication of these samples, and some results were previously published [26]. Transmission and optical absorption measurements were performed by UV-Vis spectrophotometry between 200 and 800 nm (Varian Cary 100 Scan UV-Vis spectrophotometer). All electrical measurements were performed using a voltage-current source (Keysight Agilent B2901) where, for the upper electrode, a Pt tip with ~200 μm in diameter was attached to a rod with micrometric displacement for a better approximation of the sample surface. The lower electrode (ITO) was grounded in all measurements. For realization of the measurements under illumination and dark conditions, a dark chamber was home built. A violet LED was coupled 1 cm away from the sample surface; this distance was suitably selected, aiming to provide a better homogeneity in the sample illumination where the Pt probe electrode would be acting. In addition, IR heating is minimized.

3. Structural and optical properties

Previously published [26] X-ray diffraction analyses showed hexagonal crystalline phase formation with a wurtzite ZnO structure where the films grew preferably along the axis *c* perpendicular to the substrate in direction (002). No phases corresponding to Al were identified, indicating possible incorporation of Al^{3+} ions in place of Zn^{2+} without altering the structure. This agreed with the results of RBS, confirming the structure ITO/ZnO/ZnO-Al [26, 27]. The nonidentification of crystalline phases of Al may be relevant for the construction of a device in which the insertion of the metal ion may favor the electric conduction without reducing the transparency and enabling the memristive behavior.

The transmittance and absorbance spectra are shown in **Figure 1a** and **b**. The transmittance of the glass is given for reference only. The glass/ITO substrate presents an average transmittance, in the visible region, of 90%, while the ZA1, ZA2, and ZA3 films show transmittance of ~88, 80, and 79.8%, respectively, and have absorption bands at wavelengths of 350–650 nm. This indicates that the investigated thin films exhibit excellent optical properties in the visible and near-infrared region and are semiconductors suitable for applications in electronic devices [28].

The values of the optical bandgap (E_g) were estimated using the Tauc relation in Eq. (1) [29]:

$$(\alpha h\nu)^2 = A\left(h\nu - E_g\right)^n \quad (1)$$

where A is a constant, α is the absorption coefficient, ν is the frequency of incident photons, h is the Planck constant, and E_g is the optical bandgap, which is associated with direct (n = 2) and direct (n = 1/2) transitions [28]. Adjustment was performed by linear extrapolation $(\alpha h\nu)^2 = 0$, and the graph was plotted with relation to $(\alpha h\nu)^2$ vs. E. The bandgap energy values of the samples are shown in **Figure 2** and **Table 1**. The bandgap energy obtained for the pure ITO was 3.75 eV, and the deposited films ZA1, ZA2, and ZA3 are in the range of 3.26, 3.23, and 3.19 eV, respectively. The bandgap reported in the literature for ZnO, Al-doped ZnO, and ITO is ~3.37, 3.28, and 4.2 eV, respectively [30–33]. It is important to note that in the ITO/ZnO/ZnO-Al thin films, an increase of the bandgap energy is observed with the increased thickness of the ZnO layer. This behavior depends on some process parameters such as crystallinity, grain size, and charge carrier density, which significantly affect bandgap energy [32, 34]. However, it is believed that for a greater thickness of the ZnO layer (Al poor region), the proportional number of defects that create traps between the valence band (VB) and the conduction band (CB) is smaller, resulting

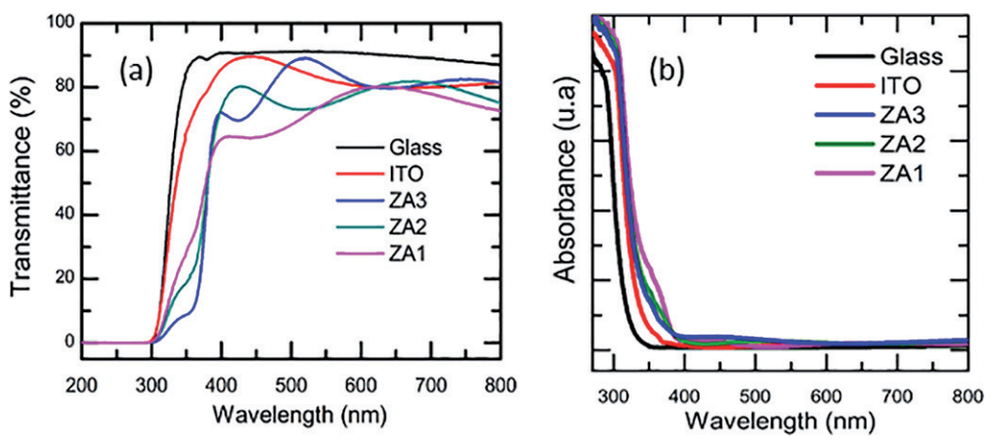

Figure 1.
(a) Transmittance and (b) absorbance spectra for ZA1, ZA2, ZA3 (ITO/glass substrate contributions were removed), ITO, and glass.

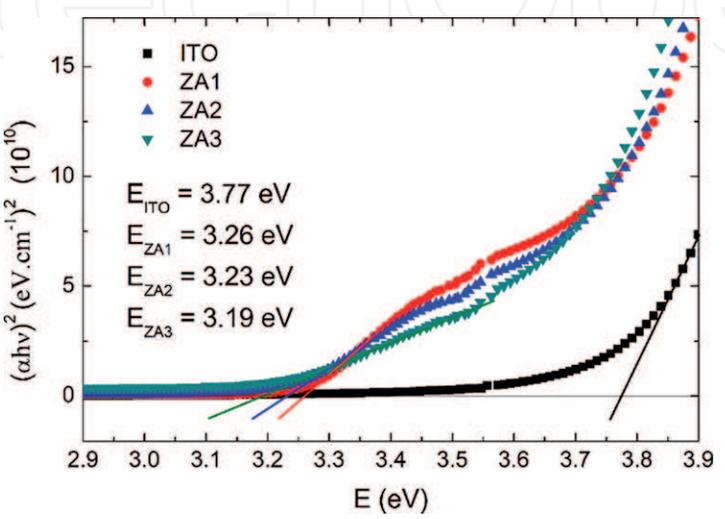

Figure 2.
Plots of $(\alpha h\nu)^2$ vs. energy of all ZnO/ZnO-Al and ITO substrates.

Thin film	Time deposition ZnO layer (min)	Thickness (nm)	Bandgap (eV)
ITO	—	100	3.77
ZA1	100	150	3.26
ZA2	60	110	3.23
ZA3	40	90	3.19

Table 1.
Optical properties of thin films of ITO/ZnO/AZO.

in a higher bandgap energy. However, for low ZnO thicknesses, the influence of the Al-rich region becomes relevant. Therefore, the number of energy levels between the VB and CB is higher, resulting in a lower average bandgap energy value. It is important to note that defects caused by the presence of Al metal forming an Al-rich ZnO (ZnO-Al) region, which may create energy levels within the bandgap, increase the availability of charge carriers over the sample when the photons impinge, thus reducing the electrical resistance.

4. Memristor behavior under dark and illumination

The memristor behavior as a function of the incidence violet light is presented in **Figure 3a**, where voltage sweeps between 0 and 2 V occurred five times and then five other sweeps between 0 and −5 V. The first five sweeps for the positive voltage polarity with the five negative polarity sweeps were performed under illumination of the violet LED (Illumination 1). Then, the same sweeping scheme was imposed on the sample; however, without ambient light (dark 1), the dark chamber was used to provide this situation. In total, the same sample was subjected to 10 alternating sweeps between illumination and dark. Observing specifically the first sweep under illumination, an adaptive-like response was found, in which the maximum value of the measured current intensity gradually increased, indicating that the electrical resistance of the sample decreases as the sweep occurs. This type of behavior is widely known in the scientific literature as the fingerprint of a memristor, where a

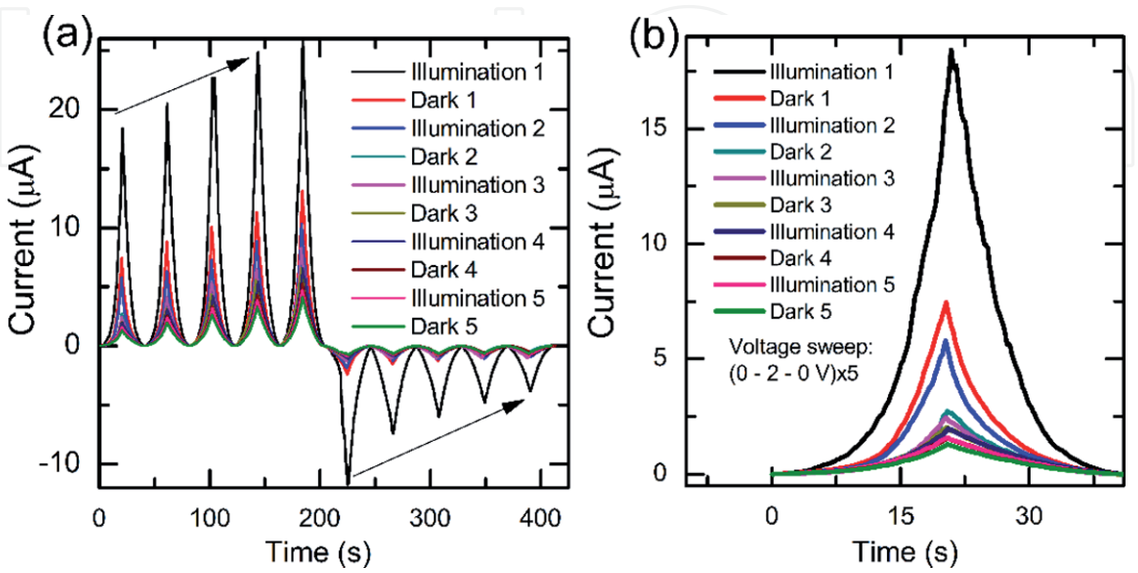

Figure 3.
(a) I–V characteristic curves of the ZA1 sample under continuous voltage scans (0 – 2 – 0 V) × 5 – (0 – (−2) – 0 V) × 5 under violet LED illumination and under darkness and (b) highlight of the first sweep cycles (0 – 2 – 0 V) × 5 under illumination and darkness.

device constructed in the form of metal-insulator (semiconductor)-metal presents electrical resistance dependent on the history of excitation by the application of an external electric field [1, 7, 26, 35].

The gradual conductivity increasing with the application of voltage is a desirable aspect related to memristors, as the memory effect associated to these devices is based on a change in the resistance state, usually a higher resistive state R_{OFF} and lower resistive states, reaching a minimum resistance level at R_{ON} [5, 8, 36]. Computational logic states are, therefore, associated with these two values of electrical resistance (bit 0—R_{OFF}; bit 1—R_{ON}). However, in this type of application, the memristors commonly present filamentary resistive switching mechanisms, where a conductive filament is formed by connecting one electrode to another [5, 6, 37]. The samples analyzed in this chapter are mechanisms based on a homogeneous resistive switching, in which electrical resistance states are gradually modified and controlled [26, 36, 38]. In this type of homogeneous resistive switching, it is possible to note an adaptive character to the applied electric voltage in which the state of resistance at a given instant depends on the entire history of the voltage sweep. Jo et al. presented a very interesting aspect of adaptation to the voltage in memristors of Si/Si + Ag thin films which behaved in a way similar to biological synaptic neurons, in other words, a neuromorphic behavior [7]. The samples worked in this chapter presented results of adaptation to voltage sweep very similar to Si/Si + Ag thin films; however, this work focused on the influence of violet LED light on memristive behaviors.

It is interesting to note that the sample showed a behavior of gradually increasing conductivity under illumination and darkness in all the sweeps. In addition, in the negative polarity, the reverse effect of decreasing conductivity was observed. These behaviors as memristors are explained in materials such as ZnO/ZnO-Ag, ZnO/ZnO-Al, or WO_3/Ag by ionic migrations through the insulating lattice [7, 26, 39]. As theoretically demonstrated by Strukov et al. [36], initially, a device with thickness D (distance between electrodes) presents maximum resistance R_{off}; however, the device may be constructed with a dopant-rich region that can continuously modulate the total resistance between R_{off} and R_{on} through ionic migrations. The control of the ionic migrations and, therefore, the resistance values reached by the device can be obtained with the application of electric voltage $V(t)$. The boundary separating the dopant-rich region from the poor region moves as a function of the applied voltage, which can cause diffusion of the ions, and the normalized position ($w(t)$) of this boundary can have values assigned between 0 and 1, where 0 refers to the case where the resistance is maximal (R_{off}) and 1 to the minimum resistance (R_{on}). Previous work has already shown that this typical behavior of the current in a memristor can be characterized as Eq. (2):

$$I(t) = \frac{1}{R_{on}w(t) + R_{off}(1 - w(t))}V(t) \tag{2}$$

where a pinched hysteresis loop can be obtained [1, 7, 26, 36, 40].

Characteristic I-V curves for different voltage frequencies were published previously in [26]; when voltage excitation frequency is diminished, the step between one conduction state and another is increased. This behavior is typical of memristor and was theoretically predicted by Chua [1] which showed that as the excitation frequency tends to infinity, the area under the I-V curve tends to zero: the effect of adaptation to the excitation is decreased dramatically. On the other hand, when the frequency is reduced, the mechanism of adaptation is evidenced. The work presented in this chapter used a fixed frequency of 5 Hz (or 200 ms excitation period) in all sweeps and samples; on this frequency, an adaptive behavior was very well observed.

The *I-V* characteristic curves under illumination present higher current values under the same voltage sweep than the dark response (see **Figure 3b**). This result indicates that the incidence of photons can significantly alter the number of free charge carriers in the CB, favoring the decrease of the electrical resistance. In this case, electrons trapped at energy levels between the VB and CB are excited due to the incidence of photons, increasing the electron population in the CB, which reduces the electrical resistance, a fact evidenced also in the bandgap values of these samples. However, as new voltage sweeps occur alternately between illumination and darkness (Illumination 1 → Dark 1 → Illumination 2 → Dark 2 → ...→Dark 5), a gradual increase in resistance is observed (decrease of the current intensity generated by the same voltage scanning interval). When the first sweep is initiated, the ion diffusion

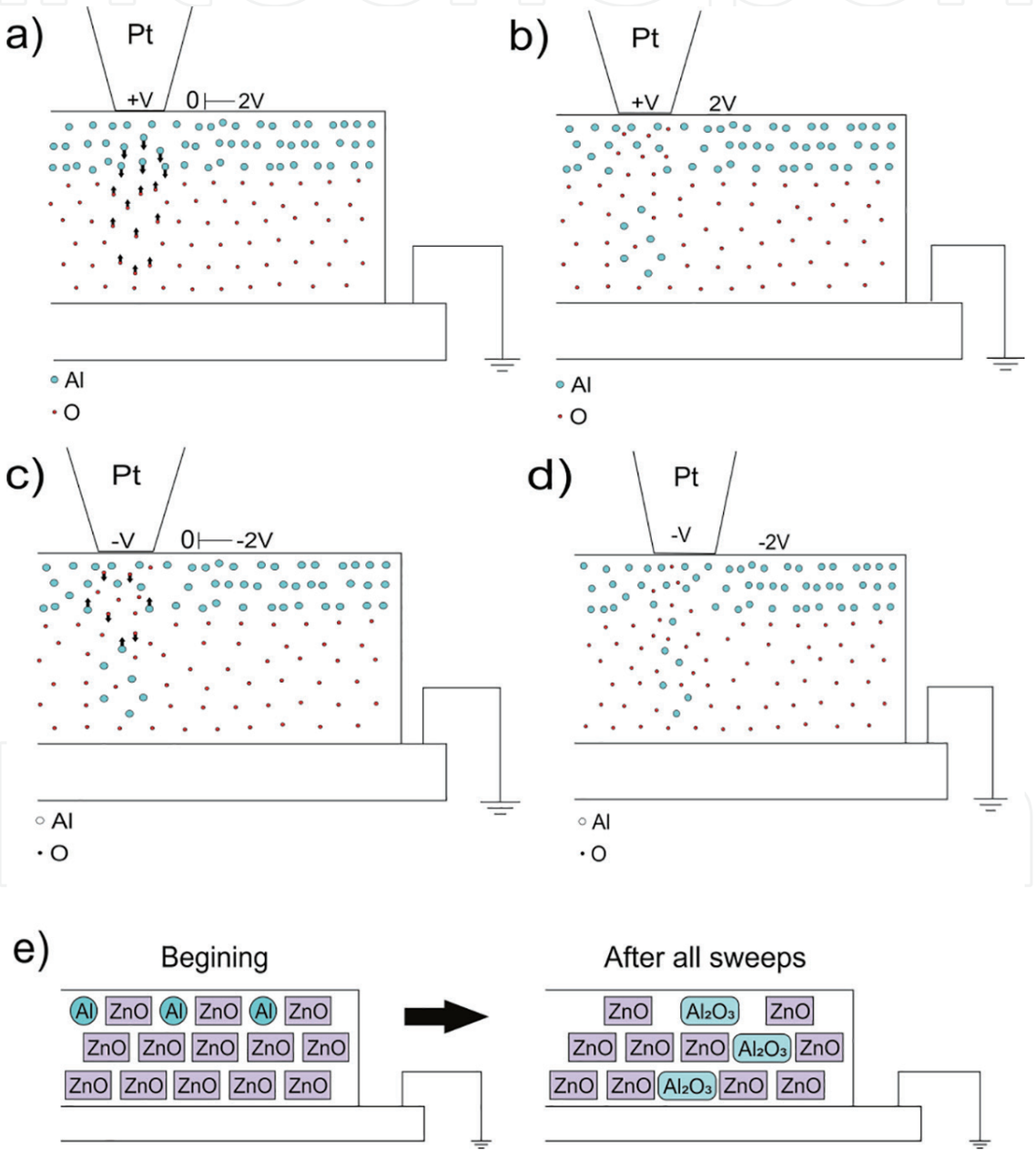

Figure 4.
Diffusion scheme of Al and oxygen dopant ions: (a) initially the Al ions are mostly in the Al-rich region, but, when the voltage sweep is initiated, Al and O ions migrate simultaneously in opposite directions; (b) after the first five sweep for positive polarity, a higher distribution of Al can be directed to the ZnO network, and oxygen ions can be allocated in the Al-rich region; (c) and (d) possible combinations of ions O with Al or Zn ions may prevent new migrations when the polarity is reversed, which indicates a formation of Al_2O_3 oxides in addition to the present ZnO; (e) ZnO and Al distribution scheme before voltage sweeps; and (f) scheme of ZnO and Al_2O_3 oxide distribution after all sweeps.

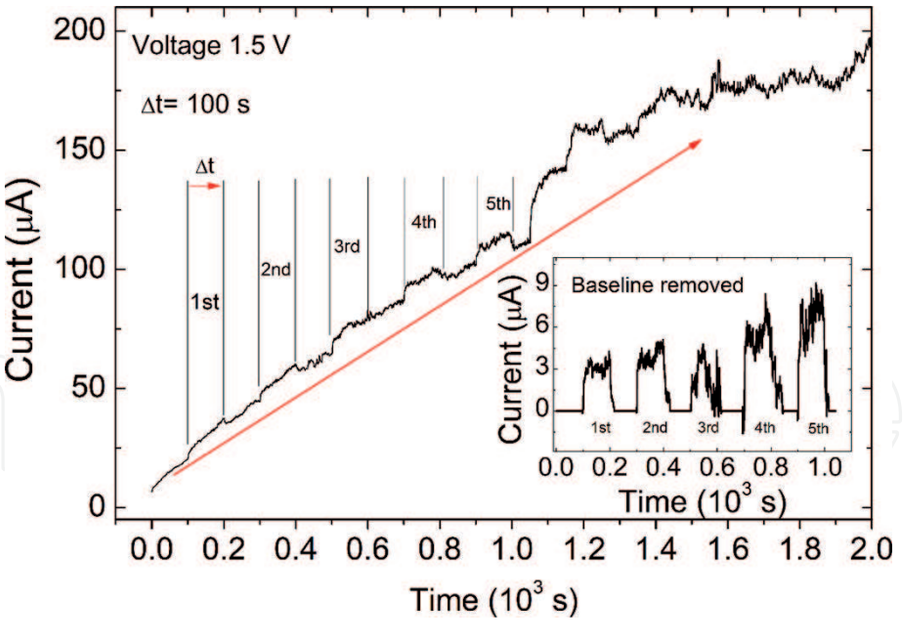

Figure 5.
Current as a function of time for a fixed voltage of 1.5 V: the red arrow indicates the direction of growth of the characteristic resistive switching current, and the violet LED light was set to oscillate between on and off at intervals Δt = 100 s; the first five light exposures are emphasized in the curve (inset: first five violet light exposures in which the baseline was removed).

process occurs, causing a distribution of Al^{3+} and O^{2-} along the entire crystalline network of the sample in a way where simultaneous migrations of Al and O ions (or oxygen vacancies) are realized. This distribution of ion dopants to the ZnO network facilitates electronic conduction, which results in the gradual decrease of the resistance, a fact known as homogeneous resistive switching [26, 38]. However, after several sweeps for positive and negative polarity, the distribution of Al and O ions enables the formation of Al_2O_3 oxide in addition to the existing ZnO network, where this fact may result in the gradual increase of the resistance after each set of voltage sweeps. **Figure 4** illustrates this ion diffusion scheme throughout the sample. Similar results were observed for samples ZA2 and ZA3 (not shown in this work).

Figure 5 shows a curve of the electric current intensity measured through the sample ZA1 as a function of the time for application of a constant voltage of 1.5 V. In each 100 s, the violet LED oscillated between on and off, where it was possible to perceive the sample response as a sensor of violet light by increasing the current intensity when illuminated for 100 s. This result is interesting because it demonstrates two simultaneous responses. The first is a homogeneous resistive switching response that indicates an adaptive process of the sample because there is no variation of the applied voltage modulus, and a gradual increase of current is observed. In addition, this memristor-like behavior is affected when the LED light is on. The first five illuminations in the sample are indicated in the inset of **Figure 5**, where the baseline has been removed. Considering that the incidence of photons in the sample can promote trapped charge carriers in the network to the CB, the amount of charge generated in the first five incidences of violet light was calculated knowing that $q = \int Idt$. The calculated electric charges were, respectively, 320.4, 420.0, 242.1, and 650.9 μC.

5. Conclusions

The ZnO/ZnO-Al thin films with memristor behavior showed a transparency of 88% in the visible region for a thickness of 150 nm, which makes it a relevant candidate in transparent electronics. The bandgap values were determined through the

optical absorption spectrum where the values are between 3.19 and 3.26 eV, similar to values in the literature for this type of material. The ZnO/ZnO-Al thin films' memristive behaviors were observed under the incidence of violet light and under darkness for cycles of voltage sweeps in which an adaptive character can be inferred. The incidence of light favored the increase of the number of carriers, but it did not impede the ion migration to form Al_2O_3 and ZnO oxides throughout the sample, a fact that gradually increased the resistance of the device. The memristor behavior was explained by the diffusion of Al ions that facilitated the electric conduction mechanism between illumination and dark conditions; however, for several voltage sweep cycles, the formation of oxides resulted in the reverse effect, increasing the resistance. Testing as a violet light sensor indicated the generation of electrical charges in the sample network while an adaptive behavior characteristic of the memristor occurred. In other words, two simultaneous phenomena were observed, in which the ZnO/ZnO-Al memristor was influenced by violet light, increasing the conductivity, at the time when it had homogeneous resistive switching due to the electric voltage. These results indicate a scientific advance in the area of resistive switching with the observation of ZnO/ZnO-Al memristive behavior dependent on the voltage application history and the ambient light conditions. In addition, new insight is provided for future research related to optical effects on memristor behaviors.

Acknowledgements

This study was financed in part by the Coordenação de Aperfeiçoamento de Pessoal de Nível Superior—Brasil (CAPES).

Conflict of interest

There is no conflict of interest.

IntechOpen

Author details

Adolfo Henrique Nunes Melo, Raiane Sodre de Araujo, Eduardo Valença and Marcelo Andrade Macêdo*
Department of Physics, Federal University of Sergipe, São Cristóvão, Sergipe, Brazil

*Address all correspondence to: odecamm@gmail.com

IntechOpen

References

[1] Chua L. Memristor—The missing circuit element. IEEE Transactions on Circuit Theory. 1971;**CT-18**:507-519. DOI: 10.1109/TCT.1971.1083337

[2] Chua LO, Kang SM. Memristive devices and systems. Proceedings of the IEEE. 1976;**64**:209-223. DOI: 10.1109/PROC.1976.10092

[3] Hu SG, Wu SY, Jia WW, Yu Q, Deng LJ, Fu YQ, et al. Review of nanostructured resistive switching memristor and its applications. Nanoscience and Nanotechnology Letters. 2014;**6**:729-757. DOI: 10.1166/nnl.2014.1888

[4] Prodromakis T, Toumazou C. A review on memristive devices and applications. In: 2010 IEEE International Conference Electronics Circuits, Systems. ICECS 2010—Proceeding; 2010. pp. 934-937. DOI: 10.1109/ICECS.2010.5724666

[5] Melo AHN, Macêdo MA. Permanent data storage in ZnO thin films by filamentary resistive switching. PLoS One. 2016;**11**:e0168515. DOI: 10.1371/journal.pone.0168515

[6] Waser R, Aono M. Nanoionics-based resistive switching memories. Nature Materials. 2007;**6**:833-840. DOI: 10.1038/nmat2023

[7] Jo SH, Chang T, Ebong I, Bhadviya BB, Mazumder P, Lu W. Nanoscale memristor device as synapse in neuromorphic systems. Nano Letters. 2010;**10**:1297-1301. DOI: 10.1021/nl904092h

[8] Yang JJ, Strukov DB, Stewart DR. Memristive devices for computing. Nature Nanotechnology. 2013;**8**:13-24. DOI: 10.1038/nnano.2012.240

[9] Szot K, Dittmann R, Speier W, Waser R. Nanoscale resistive switching in $SrTiO_3$ thin films. Physica Status Solidi Rapid Research Letters. 2007;**1**:86-88. DOI: 10.1002/pssr.200701003

[10] Mundle R, Carvajal C, Pradhan AK. ZnO/Al:ZnO transparent resistive switching devices grown by atomic layer deposition for memristor applications. Langmuir. 2016;**32**:4983-4995. DOI: 10.1021/acs.langmuir.6b01014

[11] Serrano-Gotarredona T, Masquelier T, Prodromakis T, Indiveri G, Linares-Barranco B. STDP and sTDP variations with memristors for spiking neuromorphic learning systems. Frontiers in Neuroscience. 2013;**7**:1-15. DOI: 10.3389/fnins.2013.00002

[12] Thomas A. Memristor-based neural networks. Journal of Physics D: Applied Physics. 2013;**46**:093001. DOI: 10.1088/0022-3727/46/9/093001

[13] Melo AHN, Silva PB, Macedo MA. Structural, optical, and electrical properties of ZnO/Nb/ZnO multilayer thin films. Advances in Materials Research. 2014;**975**:238-242. DOI: 10.4028/www.scientific.net/AMR.975.238

[14] Snure M, Tiwari A. Structural, electrical, and optical characterizations of epitaxial Zn_{1-x} Ga_xO films grown on sapphire (0001) substrate. Journal of Applied Physics. 2007;**101**:124912-124917. DOI: 10.1063/1.2749487

[15] Yu S, Gao B, Fang Z, Yu H, Kang J, Wong H-SP. Stochastic learning in oxide binary synaptic device for neuromorphic computing. Frontiers in Neuroscience. 2013;**7**:186. DOI: 10.3389/fnins.2013.00186

[16] Indiveri G, Linares-Barranco B, Hamilton TJ, van Schaik A, Etienne-Cummings R, Delbruck T, et al. Neuromorphic silicon neuron circuits. Frontiers in Neuroscience. 2011;**5**:1-23. DOI: 10.3389/fnins.2011.00073

[17] Indiveri G, Chicca E, Douglas R. A VLSI array of low-power spiking neurons and bistable synapses with spike-timing dependent plasticity. IEEE Transactions on Neural Networks. 2006;**17**:211-221. DOI: 10.1109/TNN.2005.860850

[18] Wu X, Xu Z, Yu Z, Sun T, Zhang T, Zhao W, et al. Resistive switching behaviors in ZnO thin films prepared by photochemical activation at room temperature. In International Photonics and OptoElectronics Meetings, OSA Technical Digest (online) (Optical Society of America). JF2A.21. 2014;3-5. DOI: 10.1364/FBTA.2014.JF2A.21

[19] Baghini MS, Kumar A. Experimental study for selection of electrode material for ZnO-based memristors. Electronics Letters. 2014;**50**:1547-1549. DOI: 10.1049/el.2014.1491

[20] Mazur M, Domaradzki J, Kaczmarek D, Moh S, Placido F. Sheet resistance and optical properties of ITO thin films deposited by magnetron sputtering with different O_2/Ar flow ratio. In International Students and Young Scientists Workshop "Photonics and Microsystems". Szklarska Poreba. 2010;60-63. DOI: 10.1109/STYSW.2010.5714168

[21] Gontijo LC, Machado R, Nascimento VP. Effects of aluminium doping on zinc oxide transparent thin films grown by filtered vacuum arc deposition. Materials Science and Engineering B. 2012;**177**:780-784. DOI: 10.1016/j.mseb.2012.02.021

[22] Li H, Chen Q, Chen X, Mao Q, Xi J, Ji Z. Improvement of resistive switching in ZnO film by Ti doping. Thin Solid Films. 2013;**537**:279-284. DOI: 10.1016/j.tsf.2013.04.028

[23] Babu BJ, Velumani S, Asomoza R. An (ITO or AZO)/ZnO/Cu(In1-xGax) Se2 superstrate thin film solar cell structure prepared by spray pyrolysis. In: IEEE; 2011. pp. 1238-1243. DOI: 10.1109/PVSC.2011.6186181

[24] Dondapati H, Santiago K, Pradhan AK. Influence of growth temperature on electrical, optical, and plasmonic properties of aluminum:zinc oxide films grown by radio frequency magnetron sputtering. Journal of Applied Physics. 2013;**114**:1-6. DOI: 10.1063/1.4824751

[25] Chen S, Lou Z, Chen D, Shen G. An artificial flexible visual memory system based on an UV-motivated memristor. Advanced Materials. 2018;**30**:1-9. DOI: 10.1002/adma.201705400

[26] Melo AHN, Valença E, Lima C, Macêdo MA. Transition from homogeneous to filamentary behavior in ZnO/ZnO-Al thin films. Journal of Alloys and Compounds. 2019;**770**:1200-1207. DOI: 10.1016/j.jallcom.2018.08.229

[27] Li X, Li H, Wang Z, Xia H, Xiong Z. Effect of substrate temperature on the structural and optical properties of ZnO and Al-doped ZnO thin films prepared by dc magnetron sputtering. Optics Communication. 2009;**282**:247-252. DOI: 10.1016/j.optcom.2008.10.003

[28] Shkir M, Arif M, Ganesh V, Manthrammel MA, Singh A, Yahia IS, et al. Investigation on structural, linear, nonlinear and optical limiting properties of sol-gel derived nanocrystalline Mg doped ZnO thin films for optoelectronic applications. Journal of Molecular Structure. 2018;**1173**:375-384

[29] Tauc J, Menth A. States in the gap. Journal of Non-Crystalline Solids. 1972;**8**:569-585

[30] Alam MJ, Cameron DC. Optical and electrical properties of transparent conductive ITO thin films deposited by sol-gel process. Thin Solid Films. 2000;**377**:455-459

[31] Sofi AH, Shah MA, Asokan K. Structural, optical and electrical properties of ITO thin films. Journal of Electronic Materials. 2018;**47**:1344-1352

[32] Aydın H, Yakuphanoglu F, Aydın C. Al-doped ZnO as a multifunctional nanomaterial: Structural, morphological, optical and low-temperature gas sensing properties. Journal of Alloys and Compounds. 2019;**773**:802-811

[33] Ou S-L, Liu H-R, Wang S-Y, Wuu D-S. Co-doped ZnO dilute magnetic semiconductor thin films by pulsed laser deposition: Excellent transmittance, low resistivity and high mobility. Journal of Alloys and Compounds. 2016;**663**:107-115. DOI: 10.1016/j.jallcom.2015.12.101

[34] Fallah HR, Ghasemi M, Hassanzadeh A. Influence of heat treatment on structural, electrical, impedance and optical properties of nanocrystalline ITO films grown on glass at room temperature prepared by electron beam evaporation. Physica E: Low-dimensional Systems and Nanostructures. 2007;**39**:69-74

[35] Kim H, Sah MP, Yang C, Roska T, Chua LO. Memristor bridge synapses. Proceedings of the IEEE. 2012;**100**:2061-2070. DOI: 10.1109/JPROC.2011.2166749

[36] Strukov DB, Snider GS, Stewart DR, Williams RS. The missing memristor found. Nature. 2008;**453**:80-84. DOI: 10.1038/nature06932

[37] Santos DAA, Zeng H, Macedo MA. Resistive switching: An investigation of the bipolar—Unipolar transition in Co-doped ZnO thin films. Materials Research Bulletin. 2015;**66**:147-150. DOI: 10.1016/j.materresbull.2015.02.051

[38] Huang CH, Huang JS, Lai CC, Huang HW, Lin SJ, Chueh YL. Manipulated transformation of filamentary and homogeneous resistive switching on ZnO thin film memristor with controllable multistate. ACS Applied Materials & Interfaces. 2013;**5**:6017-6023. DOI: 10.1021/am4007287

[39] Qu B, Du H, Wan T, Lin X, Younis A, Chu D. Materials & design synaptic plasticity and learning behavior in transparent tungsten oxide- based memristors. Materials and Design. 2017;**129**:173-179. DOI: 10.1016/j.matdes.2017.05.022

[40] Barnes BK, Das KS. Resistance switching and memristive hysteresis in visible-light-activated adsorbed ZnO thin films. Scientific Reports. 2018;**8**:1-10. DOI: 10.1038/s41598-018-20598-5